Hyperspectral Unmixing in the Presence of Mixed Noise using Joint-Sparsity and Total-Variation

Hemant Kumar Aggarwal, *Student Member, IEEE,* Angshul Majumdar, *Member, IEEE*

***Abstract*—Hyperspectral unmixing is the process of estimating constituent endmembers and their fractional abundances present at each pixel in a hyperspectral image. A hyperspectral image is often corrupted by several kinds of noise. This work addresses the hyperspectral unmixing problem in a general scenario that consider the presence of mixed noise. The unmixing model explicitly takes into account both Gaussian noise and sparse noise. The unmixing problem has been formulated to exploit joint-sparsity of abundance maps. A total-variation based regularization has also been utilized for modeling smoothness of abundance maps. The split-Bregman technique has been utilized to derive an algorithm for solving resulting optimization problem. Detailed experimental results on both synthetic and real hyperspectral images demonstrate the advantages of proposed technique.**

***Index Terms*—Hyperspectral Unmixing, Joint-Sparsity, Split-Bregman, Total Variation, Mixed-noise**

I. Introduction

HYPERSPECTRAL unmixing is a classical, important and challenging problem in remote sensing. It is a problem of identifying endmembers and their fractional abundances present at every pixel in a hyperspectral image. The term endmember refers to various materials that may be directly or indirectly present in a hyperspectral image. The term direct presence refers to the existence of pure pixels and indirect presence refers to mixed pixels. A pixel in a satellite image corresponds to an extensive spatial area on earth. This spatial region constituting that pixel may be covered by a single object or multiple objects. If the area covered by a pixel constitutes a single object then such a pixel is called pure pixel otherwise it is called mixed pixel. The term fractional abundance indicates the percentage of a particular endmember present at a pixel. Thus, abundance map shows the distribution of a particular endmember over a region. The pure pixels have the fractional abundance of one whereas mixed pixels have fractional abundance between zero and one.

Hyperspectral unmixing has applications in various domains such as geology, agriculture [1], environmental studies, biology [2], etc. The abundance maps are often used as feature vectors [3] in several image processing and pattern recognition related applications of hyperspectral images. Hyperspectral unmixing is also used in denoising [4], data fusion [5], and super-resolution [6] related applications.

If a hyperspectral image is of very high resolution, then its constituent endmembers shall be considered at micro level such as chemical composition of the pixel. These images require the unmixing problem to be handled at the micro level. However in this work we are interested in the macro level decomposition of a pixel into its constituent components. An overview of hyperspectral unmixing algorithms has been discussed in [7]. This work is based on linear mixing model for unmixing, however, there are various nonlinear models for the hyperspectral unmixing whose survey can be found in [8]. There are algorithms such as pixel purity index (PPI) [9] and N-FINDER [10] which require presence of pure pixels in the image. However this assumption may not be true always, and therefore, this work does not depend on this assumption. Hyperspectral unmixing approaches can also be categorized as the one that utilizes existing spectral libraries and others that try to estimate endmember spectral signatures using non-negative matrix factorization based techniques such as [11]. This work is based on utilizing existing spectral libraries available for many materials in different categories of endmembers such as artificial, minerals, soils, etc.

Often hyperspectral images are corrupted by some kinds of noise such as Gaussian noise, impulse noise, shot noise, horizontal or vertical line strips, etc. Gaussian noise mostly occurs during image acquisition process due to poor lighting, dark current or sensor noise. Horizontal line strips often occur in images captured by whisk-broom kind of sensors that have rotating mirrors perpendicular to the flight direction. Vertical line strips mostly occur in images captured by push-broom kind of sensors which capture scene along the flight direction. Shot noise occurs due to some defective pixels.

It is desirable to do unmixing of hyperspectral images even when they are corrupted by one or several of these kinds of noise. This problem of unmixing in the presence of mixed noise can be approached by firstly applying a denoising algorithm followed by the unmixing algorithm. This work directly recovers the abundance map in the presence of mixed noise. There are studies such as [4], [12] that also perform unmixing in the presence of noise. This work is different from these existing methods in terms of both the noise model and the solution approach.

This work utilizes the noise model proposed in [13] which was later utilized for denoising in [14]. This model allows us to formulate the linear hyperspectral unmixing problem that explicitly account for both Gaussian and sparse noise. The term sparse noise corresponds to the noise that affects few pixels in the image. It includes line strips, shot noise as well as impulse noise. The total number of endmembers available from different spectral libraries (e.g. the USGS library) are huge, but only a few of these endmembers are present in a given hyperspectral image. At every pixel, a subset of the

Hemant Kumar Aggarwal and Angshul Majumdar are associated with Indraprastha Institute of Information Technology-Delhi, India. Hemant Kumar Aggarwal is supported by TCS research fellowship.

endmembers (present in the whole image) are present This observation can be modeled as joint-sparse [15] regularization on abundance maps. Natural images often exhibit high spatial correlation implying that pixels having the same spectral signature may be present in the neighborhood. This observation can be modeled as total-variation [16] regularization on abundance maps. Thus, this work proposes a hyperspectral unmixing algorithm that utilize generic noise model and explores both joint sparsity and spatial smoothness of abundance maps. The resulting optimization problem is solved using the split-Bregman [17] based technique. Our work improves over the state of the art sparse regression based unmixing techniques sparse regression (SR) [18] and its variants total variation spatial regularization (SRTV) [19] and collaborative sparse regression (CLSR) [20].

Section II describes detailed problem formulation followed by section III where we discuss the technique to solve proposed formulation. Section IV describes experimental results and section V concludes the paper with some future directions.

II. Problem Description and Formulation

This section describes how linear unmixing problem can be mathematically formulated as sparse recovery problem followed by our proposed problem formulation.

A. Notations

Let I_n represents identity matrix of size $n \times n$. The operation $x = vec(X)$ represents vectorization operation on matrix X with columns appended whereas $X = mat(x)$ represents its inverse operation. A hyperspectral datacube of size $m \times n \times b$ can be represented as a matrix of size $b \times p$ where b is the total number of bands and $p = m \times n$ is the total number of pixels in the image. $M \in \mathbb{R}^{b \times e}$ represents mixing matrix also called endmember matrix in which each column represents spectral signature of an endmember. Let $\nabla = \begin{pmatrix} \nabla_h \\ \nabla_v \end{pmatrix}$ be total variation operator with ∇_h and ∇_v representing horizontal and vertical total variation operators respectively with $(\nabla_h X)_{i,j} = X_{i,j+1} - X_{i,j}$ and $(\nabla_v X)_{i,j} = X_{i+1,j} - X_{i,j}$. The $\ell_{2,1}$ norm of a matrix $A \in \mathbb{R}^{M \times N}$ is defined as

$$\|A\|_{2,1} = \sum_{i=1}^{M} \|a_i^{\rightarrow}\|_2 = \sum_{i=1}^{M} \sqrt{\sum_{j=1}^{N} a_{ij}^2}$$

whereas Frobenius norm and ℓ_1 norm of a matrix are defined as follows

$$\|A\|_F^2 = \sum_{i=1}^{M}\sum_{j=1}^{N} a_{ij}^2, \quad \|A\|_1 = \sum_{i=1}^{M}\sum_{j=1}^{N} |a_{i,j}|.$$

B. Problem Description

The linear unmixing problem for a pixel in the presence of Gaussian noise is represented as constrained linear regression model:

$$y = Ma + n, \quad \|a\|_1 = 1, \quad a_i \geq 0 \; \forall i \tag{1}$$

where $y \in \mathbb{R}^{b \times 1}$ is a pixel vector in b spectral bands, M is a mixing matrix with e number of endmembers as column vectors, $a \in \mathbb{R}^{e \times 1}$ is called abundance vector that represents the fraction of each endmember used in the formation of that pixel, and n represents Gaussian noise which accounts for various external environmental factors. The constraint $\|a\|_1 = 1$ represents abundance sum-to-one constraint to ensures that total contribution of each endmember in formation of a pixel is one. As it has been noticed in [7], [21], [22], all the endmembers present in a real hyperspectral image may not be available in the spectral library. Therefore, abundance sum may not be exactly equal to one. Also, if this constraint of $\|a\|_1 = 1$ is enforced then formulating the ℓ_1-norm minimization problem on a will be meaningless. Therefore, this work does not enforce this constraint in the problem formulation. The abundance non-negativity constraint represents that contribution can not be negative.

Since mixing matrix is known for hundreds of most commonly used materials. Therefore generally $e > b$ and (1) is an underdetermined system of linear equations. In general, an underdetermined system has infinite solutions therefore, we need additional constraints on the variable a to determine it uniquely. The observation that a pixel is mixture of very few endmembers as opposed to hundreds of available endmembers allow us to treat abundance vector a as sparse vector thus unmixing can be recast as compressed sensing [23], [24] problem :

$$\min_a \|y - Ma\|_2^2 \text{ subject to } \|a\|_0 \leq k \tag{2}$$

where k is the sparsity of a i.e. maximum number of non-zero elements of a. This is an NP-hard [25] problem whose solution can be approximated using greedy pursuit algorithms such as OMP [26], StOMP [27], CoSAMP [28], etc. It has been shown that under certain conditions solution of the NP-hard problem (2) can be approximated by solving its convex surrogate ℓ_1-norm minimization problem

$$\min_a \|y - Ma\|_2^2 + \lambda \|a\|_1. \tag{3}$$

This problem is a convex optimization problem, and various algorithms have been proposed in literature SPGL1 [29], FISTA [30], NESTA [31], Bregman Iteration [32], etc., to solve this problem. The unmixing model in (1) can be extended for all the pixels as

$$Y = MA + N, \quad A \geq 0 \tag{4}$$

where $Y \in \mathbb{R}^{b \times p}$ is a matrix with p pixels as column vectors, $A \in \mathbb{R}^{e \times p}$ is sparse abundance matrix, N is Gaussian noise. This unmixing model can be though of as specialization of image denoising model :

$$Y = X + N$$

where $X \in \mathbb{R}^{b \times p}$ and $X = MA$ is clean hyperspectral image which imply that unmixing can lead to denoising provided that mixing matrix is known.

C. Proposed Formulation

A real hyperspectral images may contain a mixture of Gaussian and sparse noise therefore, we consider the mixed noise model for unmixing and account for both types of noise. The usual unmixing model in (4) can be extended as

$$Y = MA + S + G, \quad A \geq 0 \tag{5}$$

here S and G represents sparse and Gaussian noise respectively. The above noise model assumes both Gaussian and sparse noise to be additive noise. Sparse noise accounts for horizontal or vertical line strips, shot noise and any impulse noise present in a hyperspectral image. All these kinds of noise are termed as sparse noise since they corrupt few pixels in a hyperspectral image. By utilizing this model, we can formulate the unmixing problem as:

$$\min_{A,S} \|Y - MA - S\|_F^2 + \lambda_1 \|A\|_{2,1} + \lambda_2 \|S\|_1 \tag{6}$$

Here the first term is data fidelity term that is equivalent to minimizing the variance of Gaussian noise $G = Y - MA - S$. First regularization term is an $\ell_{2,1}$-norm minimization term on abundance matrix A which is also called joint-sparse regularization term. This term is based on the observation that in most hyperspectral images, a fewer endmembers are present compared to the available endmembers. This observation is mathematically modeled as joint-sparse regularization on matrix A with few non-zero rows, but each non-zero row is allowed to be dense. The second regularization term corresponds to minimizing ℓ_1-norm of sparse noise matrix S. Here ℓ_1-norm is minimized due to modeling assumption that sparse noise affects few pixels in the image.

As an alternative unmixing model, we can also exploit the fact that most natural images are piece-wise smooth e.g. if there are some vegetation pixels in the image the nearby pixels are also likely to be vegetation pixels. Therefore, the abundance maps can be considered as piece-wise smooth. The piece-wise smoothness can be modeled as total variation regularization [16].

$$\min_{A,S} ||Y - MA - S||_F^2 + \lambda_1 ||\nabla A^T||_1 + \lambda_2 \|S\|_1 \tag{7}$$

Here ∇ is two-dimensional total variation operator that applies total variation along both horizontal and vertical direction on a 2D image. The operator ∇ is applied on A^T because each abundance map is along rows of A.

In this work, we propose to simultaneously exploit both the joint-sparsity as well as spatial smoothness of the abundance maps in the light of generic noise model. Thus the proposed hyperspectral unmixing problem formulation can be expressed as:

$$\min_{A,S} ||Y - MA - S||_F^2 + \lambda_1 ||\nabla A^T||_1 + \lambda_2 \|A\|_{2,1} + \lambda_3 \|S\|_1 \tag{8}$$

here λ_1, λ_2 and λ_3 are regularization parameters corresponding to total-variation term, joint-sparsity term, and sparse noise term respectively. These three models in (6), (7), and (8) estimates sparse noise S as a byproduct of the proposed formulations. Let $X = MA$ be the clean image then we can get denoised image $\hat{X} = M\hat{A}$ where $\hat{A}$ is the estimated abundance maps by solving (8). Along with generic noise model (5), we have exploited both joint-sparsity as well as piecewise-smoothness of abundance maps. We are not aware of any efficient algorithm to solve (8) therefore in the next section we briefly describe how to solve this problem using the split-Bregman [17] based technique.

III. Proposed Algorithm

This section describes how the split-Bregman [17] approach can be utilized to derive the algorithm for solving (8). The split-Bregman approach is suitable to solve (8) because it has been designed to handle multiple regularization terms.

The variable A is not separable in (8) therefore we utilize auxiliary variables P and Q to make the problem separable. Set $P = \nabla A^T$ and $Q = A$, then we get following constrained problem:

$$\begin{aligned} \underset{A,S,P,Q}{\text{minimize}} \quad & \|Y - MA - S\|_F^2 + \lambda_1 \|P\|_1 + \lambda_2 \|Q\|_{2,1} + \lambda_3 \|S\|_1 \\ \text{subject to} \quad & P = \nabla A^T \\ & Q = A \end{aligned}$$

This problem can be re-written into unconstrained form by using two Bregman variables B_1 and B_2 to get

$$\begin{aligned} \underset{A,S,P,Q}{\text{minimize}} & \|Y - MA - S\|_F^2 + \lambda_1 \|P\|_1 + \lambda_2 \|Q\|_{2,1} + \lambda_3 \|S\|_1 \\ & + \mu_1 \|P - \nabla A^T - B_1\|_F^2 + \mu_2 \|Q - A - B_2\|_F^2 \end{aligned}$$

where B_1 and B_2 are updated as:

$$\begin{aligned} B_1 &= B_1 + \nabla A^T - P \\ B_2 &= B_2 + A - Q \end{aligned}$$

Above problem is separable in each variable therefore can be written into following subproblems as

$$\begin{aligned} \text{P1}: \quad & \min_P \ \mu_1 \|P - \nabla A^T - B_1\|_F^2 + \lambda_1 \|P\|_1 \\ \text{P2}: \quad & \min_Q \ \mu_2 \|Q - A - B_2\|_F^2 + \lambda_2 \|Q\|_{2,1} \\ \text{P3}: \quad & \min_S \ \|Y - MA - S\|_F^2 + \lambda_3 \|S\|_1 \\ \text{P4}: \quad & \min_A \ \|Y - MA - S\|_F^2 + \mu_1 \|P - \nabla A^T - B_1\|_F^2 \\ & \qquad + \mu_1 \|Q - A - B_2\|_F^2 \end{aligned}$$

each of these problems can be solved iteratively by using Bregman iteration with Bregman variables updated in k^{th} iteration as

$$\begin{aligned} B_1^{k+1} &= B_1^k + \nabla (A^k)^T - P^k \\ B_2^{k+1} &= B_2^k + A^k - Q^k \end{aligned}$$

The problems $P1$ and $P3$ are of the form

$$\|y - x\|_2^2 + \lambda \|x\|_1$$

which can be solved by using soft-thresholding [33] operation:

$$\hat{x} = \text{SoftTh}(y, \lambda) = \text{sign}(y) \times \max \left\{ 0, |y| - \frac{\lambda}{2} \right\},$$

The problem $P2$ can be solved by using the procedure as described in section 3.3.3 of [15]. This is a ℓ_2-norm shrinkage operation on each row $q^{(i)}$ $\forall i = 1, 2 \dots e$, of matrix Q. The ℓ_2-norm shrinkage problem is

$$\min_x \|y - x\|_2^2 + \lambda \|y\|_2$$

whose solution is given by

$$\hat{x} = \text{Shrink}(y, \lambda) = \max\left\{\|y\|_2 - \frac{\lambda}{2}, 0\right\} \odot \frac{y}{\|y\|_2},$$

here $\odot$ represent element by element multiplication operation with the assumption that $0 \times \frac{0}{0} = 0$. The problem $P4$ is a differentiable convex optimization problem. After differentiating we get following linear system of equations with variable A :

$$\begin{aligned} M^T M A + \mu_1 A \nabla^T \nabla + \mu_2 A = M^T (Y - S) \\ + \mu_1 (P^T - B_1^T) \nabla + \mu_2 (Q - B_2) \end{aligned}$$

this equation can be re-written as

$$\begin{aligned} \Psi a =& vec(M^T (Y - S)) + \alpha \quad \text{where} \\ \Psi =& (I_e \otimes M^T M) \mu_1 (\nabla^T \nabla \otimes I_e) + \mu_1 I_{pe} \\ \alpha =& \mu_1 (P^T - B_1^T) \nabla + \mu_2 (Q - B_2)) \end{aligned} \tag{9}$$

The above system of linear equations is large and sparse whose solution can be approximated using algorithms such as LSQR [34]. Algorithm 1 outlines the steps of proposed jointly-sparse and total-variation regularized hyperspectral unmixing algorithm using the split-Bregman approach. We use the acronym JSTV for the proposed Joint Sparsity and Total Variation based unmixing method. By setting $\lambda_1 = 0$, we can derive the solution of (6) which we refer as Split-Bregman algorithm based Joint-Sparse regularized (SBJS) unmixing algorithm. Similarly $\lambda_2 = 0$ results in an algorithm that solves (7) which we refer as Split-Bregman algorithm based Total-Variation regularized (SBTV) unmixing algorithm.

Algorithm 1 Proposed JSTV Algorithm for solving (8)

input: Y, λ_1, λ_2, μ_1, μ_2, innerIter, outerIter
output: $\hat{A}$ (Abundance maps).
for $j = 1$ to outerIter **do**
  for $k = 1$ to innerIter **do**
    $P^{k+1} = \text{SoftTh}(\nabla (A^k)^T + B_1^k, \frac{\lambda_1}{\mu_1})$
    $Q^{k+1} = \text{Shrink}(A^k + B_2^k, \frac{\lambda_2}{\mu_2})$
    $S^{k+1} = \text{SoftTh}(MA^K - Y, \lambda_3)$
    $A^{k+1} = \text{mat}(a)$ from (9)
    $B_1^{k+1} = B_1^k + D_h X^{k+1} D - P^{k+1}$
    $B_2^{k+1} = B_2^k + D_v X^{k+1} D - Q^{k+1}$
  end for
  $Y = Y - MA^k - S^k$
end for
return $\hat{A} = A^{j+1}$

IV. Experiments and Results

This section describes the details of various experiments executed to validate the proposed method. Firstly datasets used in the experiments are described followed by evaluation metrics. After that, various synthetic data experiments and real data experiments are detailed with analysis of results.

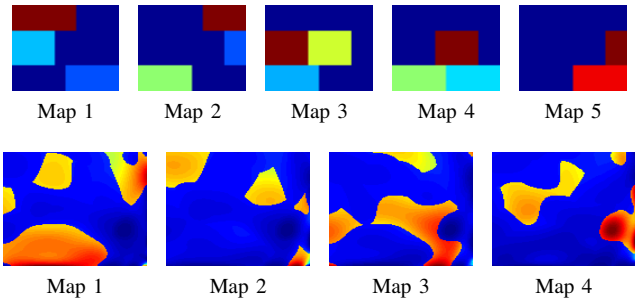

Fig. 1. Row one shows five synthetically generated abundance maps corresponding to first synthetic image whereas row two shows four abundance maps corresponding to second synthetic image.

A. Data Description

The existing USGS spectral library [35] was utilized in all the experiments. The library contains spectral signatures under six categories namely artificial, coatings, minerals, liquids, soil, and vegetation. We utilized endmembers from each of these categories in the experiments. We manually checked each endmember signature and removed some of the endmembers that had missing values for some wavelengths.

Experiments were conducted with two synthetic and one real dataset. The first synthetic dataset has five abundance maps of 50×50 pixels with constant fraction value over a region. These abundance maps are shown in row one of Fig. 1. Each abundance map is composed of two or three endmembers as represented by the number of rectangular boxes inside a map. Dark blue background color represents zero pixel value. Five endmembers were randomly selected to generate first synthetic image of dimension $50 \times 50 \times 224$. The second synthetic dataset was generated using HYDRA toolbox [36]. Four abundance maps of size 128×128 were generated using Legendre method and are shown in row two of Fig. 1. The second synthetic image of dimension $128 \times 128 \times 224$ was generated using four randomly selected endmembers from the spectral library. Both the datasets satisfy abundance sum to one constraint as well as abundance non-negativity constraint.

The experiments on the first synthetic image were conducted with the endmember matrix of dimension $\mathbb{R}^{224 \times 269}$ such that angle between any two spectral signatures was at least 4 degree. The experiments with second synthetic image does not make any such assumption and utilized endmember matrix of dimensions $\mathbb{R}^{224 \times 889}$.

Real data experiments were done with a portion of Jasper Ridge image [37] of size $112 \times 118 \times 224$. A false color composite image is shown in Fig. 2. Several bands in this image are noisy bands. We had considered all 224 bands in real data experiments as opposed to many unmixing algorithms that remove noisy bands before doing unmixing. We did not have actual abundance maps for this real dataset however four major constituent endmembers can be easily recognized by visual interpretation. These four endmembers are roads, vegetation, soil and water as indicated in the Fig. 2.

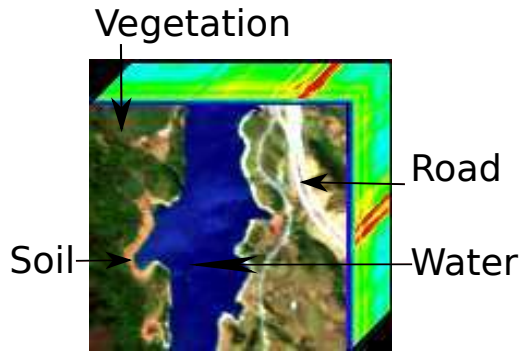

Fig. 2. Portion of Jasper image used in experiments.

B. Synthetic Data Experiments

The synthetic data experiments were conducted to quantify the performance of proposed unmixing algorithm.

All three variables (B_1, B_2, S) required by our algorithm were initialized to zero. Each of the endmember in the matrix M was normalized by ℓ_2-norm. The abundance matrix A was initialized with random values such that they satisfy both the abundance sum constraint as well as the non-negativity constraint. The parameters λ_1, λ_2, λ_3, control the strength of smoothness, joint-sparsity and sparse noise term respectively. If the parameter values are zero then there is no denoising/unmixing and output is same as input. As we increase any parameter's value then that regularization term will be in effect. For example, a higher value of λ_1 will enforce resulting abundance maps to be highly joint sparse and it will trade-off with retaining original abundance maps. Similarly, a higher value of λ_2 will encourage results with low total variation of abundance maps. Increasing the value of λ_3 will promote results with low sparse noise. However, after a limit, high values of parameters tend to deviate resulting outputs image from original image.

The values of parameters for synthetic experiments were found experimentally using five-fold cross validation. The values for proposed JSTV algorithm used in experiments are $\lambda_1 = 2, \lambda_2 = 0.1, \lambda_3 = 1, \mu_1 = 0.04, \mu_2 = 1$. Parameter values of SBTV algorithm were found to be $\lambda_1 = 0.05, \lambda_2 = 0, \lambda_3 = 1, \mu_1 = 0.05, \mu_2 = 0$. Parameter values for SBJS algorithm were found to be $\lambda_1 = 0, \lambda_2 = 1, \lambda_3 = 1, \mu_1 = 0, \mu_2 = 2$. The parameters required by SR, SRTV, and CLSR algorithms were set as described in corresponding articles. In particular, parameter value of $\lambda = 5e^{-4}$ was used in SR algorithm. $\lambda = 3e^{-3}, \lambda_{TV} = 0.01, \mu = 0.01$ were used in SRTV algorithm and $\lambda = 1.3e^{-3}$ was used in CLSR algorithm. The two parameters of LRMR algorithm, rank and sparsity, were set to 8 and 15000 respectively. As the noise changes we need to adjust values of these parameters accordingly; however, the split-Bregman algorithm is quite robust to small changes in parameter values.

The first set of experiments was done to check the robustness of proposed unmixing method in the presence of different kinds of noise. Tables I and II quantifies the reconstruction quality of each method on two synthetic images using PSNR and SSIM values. The numerical values shown corresponding to each algorithm represents the average of PSNR values obtained for different abundance maps. The maximum value of PSNR and SSIM are boldfaced. Last two rows in both of these tables represent the case when mixed noise is present. This mixed noise causes a sharp decrease in performance of SR, SRTV, and CLSR algorithms because these three algorithms are not designed to handle impulse noise. The SBJS, SBTV, and proposed JSTV methods reduce that noise because of utilization of sparse noise concept in the unmixing framework. The results in Table II obtained on the second synthetic image are not quantitatively as good as the results in Table I for the first synthetic image. The main reason is the utilization of different unmixing matrices in both the cases. The endmembers matrix M in the second case was highly coherent compared to the first case.

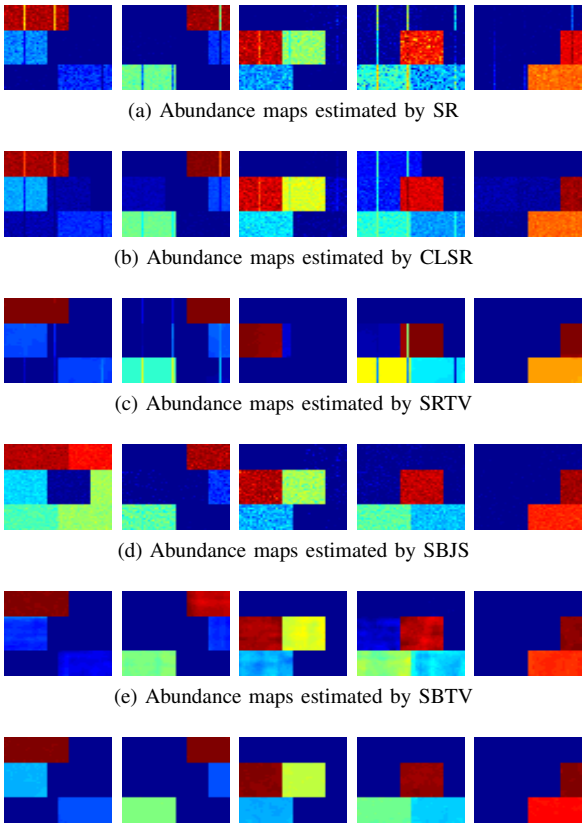

(a) Abundance maps estimated by SR

(b) Abundance maps estimated by CLSR

(c) Abundance maps estimated by SRTV

(d) Abundance maps estimated by SBJS

(e) Abundance maps estimated by SBTV

(f) Abundance maps estimated by proposed JSTV

Fig. 3. Reconstructed Abundance maps by different algorithms

The second set of experiments were done on the synthetic image with mixed noise consisting of Gaussian noise and vertical line strips. Gaussian noise of signal to noise ratio (SNR) of 30 dB was added along with three vertical line strips. The noisy image is shown in Fig. 5(b). The unmixing algorithms were run on this noisy image. The resulting abundance maps are shown in Fig. 3. It can be observed from Fig. 3(a), 3(b), and 3(c) that SR, CLSR, and SRTV are not able to remove line strips from the abundance maps; however, the SRTV algorithm has reduced Gaussian noise. The SBJS algorithm is not able to reduce Gaussian noise but has reduced line strips as observed in Fig. 3(d). The proposed JSTV algorithm has reduced both the noise from all the abundance maps as can be seen by

TABLE I
PSNR AND SSIM VALUES FOR DIFFERENT NOISE LEVELS. THE VALUES SHOWN ARE AVERAGED FOR FIVE ABUNDANCE MAPS. MIX1 CORRESPONDS TO GAUSSIAN NOISE OF SNR 30 DB AND THREE VERTICAL LINES WHEREAS MIX2 IS MIX1 + 1% IMPULSE NOISE.

Noise	Peak Signal to Noise Ratio (dB)						Structural Similarity Index (SSIM)					
SNR(dB)	SR	SRTV	CLSR	SBJS	SBTV	JSTV	SR	SRTV	CLSR	SBJS	SBTV	JSTV
40	40.21	45.77	34.23	44.36	59.08	**61.94**	0.981	0.997	0.91	0.993	0.999	**0.999**
30	29.92	37.73	33.23	32.79	42.6	**46.82**	0.847	0.989	0.957	0.869	0.981	**0.99**
20	20.52	24.37	21.16	22.27	27.5	**29.87**	0.609	0.78	0.657	0.583	0.827	**0.84**
mix1	25.25	31.19	25.23	32.65	41.58	**46.84**	0.78	0.964	0.77	0.869	0.975	**0.994**
mix2	18.79	18.57	18.89	32.39	41.71	**46.23**	0.594	0.802	0.607	0.862	0.979	**0.992**

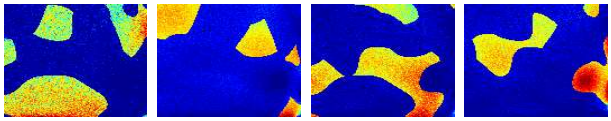

(a) Abundance maps estimated by SR

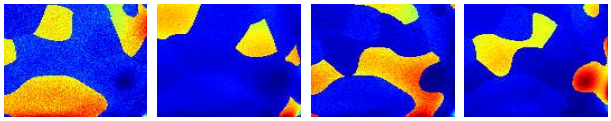

(b) Abundance maps estimated by CLSR

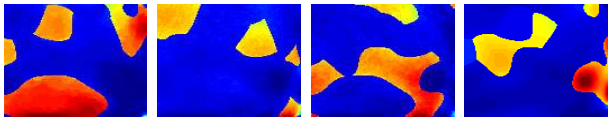

(c) Abundance maps estimated by SRTV

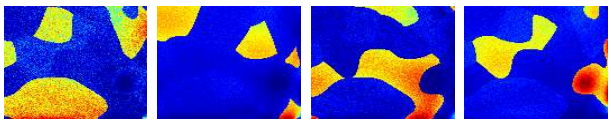

(d) Abundance maps estimated by SBJS

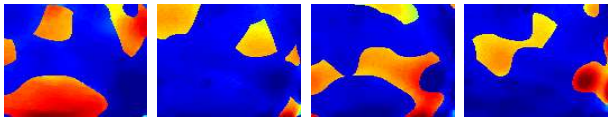

(e) Abundance maps estimated by SBTV

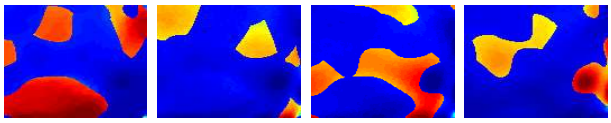

(f) Abundance maps estimated by proposed JSTV

Fig. 4. Reconstructed Abundance maps by different algorithms

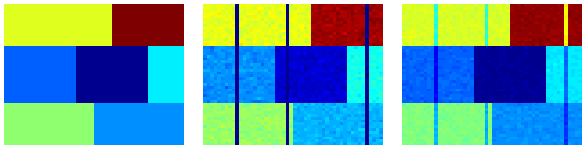

(a) Original (b) Noisy (c) SR

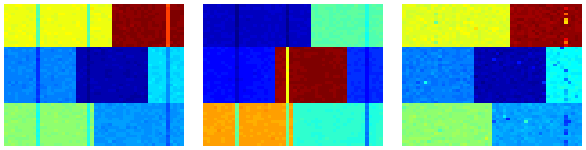

(d) CLSR (e) SRTV (f) LRMR

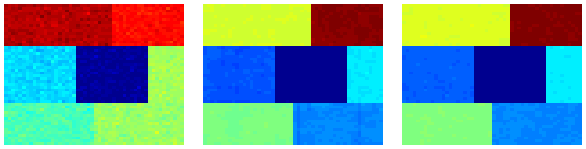

(g) SBJS (h) SBTV (i) JSTV

Fig. 5. Denoising results by different algorithms on synthetic image

comparing estimated abundance maps in Fig. 3(f) with original abundance maps shown in Fig. 1. The unmixing results on the second synthetic image in the presence of only Gaussian noise of SNR 30 dB are shown in Fig. 4. All four abundance maps recovered by each algorithm are shown in Fig. 4 because a particular unmixing algorithm may recover some abundance maps correctly while causing other abundance maps to be noisy.

The third set of experiments was carried out to check denoising capability of proposed algorithm. The denoising results have been compared with existing denoising algorithm LRMR [14] that also takes mixed noise into account. The sparse unmixing models in (4) and (5) results not only in abundance maps but can also provide denoised hyperspectral image $\hat{X}$ when estimated abundance matrix $\hat{A}$ is multiplied by endmember matrix M i.e. $\hat{X} = M\hat{A}$ where $\hat{X}$ is estimated image. The denoising results are shown in Fig. 5. The synthetically generated abundance maps were multiplied with five randomly selected endmembers to generate $50 \times 50 \times 224$ synthetic hyperspectral image whose band 1 is shown in Fig. 5(a). Figures 5(g), 5(h), and 5(i) clearly shows the advantage of utilizing the concept of sparse noise in the unmixing framework. Since this image has a lot of smooth regions therefore Gaussian noise can be easily spotted in denoised images however compared to other algorithms the proposed JSTV algorithm has significantly reduced both kinds of noise. The denoising results with the second synthetic image are shown in Fig. 6. The noisy image of Fig. 6(b) was generated with mixed noise consisting of Gaussian noise of SNR 30 dB, 1% impulse noise, and three vertical lines. The denoising results are quantified using PSNR and SSIM values that are shown in Table III. The denoised results produced by SBJS (Fig. 6(g)), SBTV (Fig. 6(h)), and JSTV (Fig. 6(i)) algorithms in the presence of mixed noise, are visually more clear compared to results produced by of SR (Fig. 6(d)), SRTV (Fig. 6(e)) and CLSR (Fig. 6(f)) since these three algorithms does not explicitly account for the presence of

TABLE II
PSNR AND SSIM VALUES FOR DIFFERENT NOISE LEVELS. THE VALUES SHOWN ARE AVERAGED FOR FIVE ABUNDANCE MAPS. MIX1 CORRESPONDS TO GAUSSIAN NOISE OF SNR 30 DB AND THREE VERTICAL LINES WHEREAS MIX2 IS MIX1 + 1% IMPULSE NOISE.

Noise	Peak Signal to Noise Ratio (dB)						Structural Similarity Index (SSIM)					
SNR(dB)	SR	SRTV	CLSR	SBJS	SBTV	JSTV	SR	SRTV	CLSR	SBJS	SBTV	JSTV
40	28.25	36.76	34.78	36.54	34.68	**43.12**	0.63	0.94	0.89	0.88	0.93	**0.98**
30	22.86	31.25	26.84	26.43	31.64	**39.21**	0.41	0.86	0.71	0.56	0.91	**0.97**
20	16.73	24.37	18.65	24.71	27.59	**25.32**	0.22	0.78	0.36	0.23	0.67	**0.74**
mix1	22.43	25.23	26.23	26.19	33.54	**38.98**	0.41	0.68	0.69	0.54	0.94	**0.97**
mix2	13.62	12.78	13.66	25.55	30.59	**38.56**	0.19	0.16	0.28	0.52	0.89	**0.97**

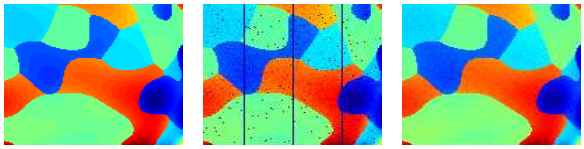

(a) Original (b) Noisy (c) LRMR

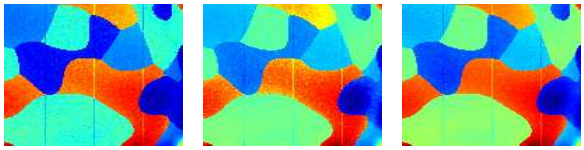

(d) SR (e) SRTV (f) CLSR

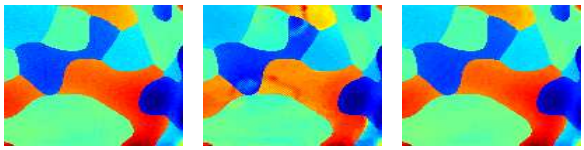

(g) SBJS (h) SBTV (i) JSTV

Fig. 6. Denoising results by different algorithms on synthetic image

TABLE III
PSNR AND SSIM VALUES FOR DENOISED SYNTHETIC IMAGE 2

	PSNR (dB)		SSIM	
Noise	LRMR	JSTV	LRMR	JSTV
40	51.12	49.39	0.99	0.99
30	42.01	43.38	0.99	0.99
20	31.57	32.36	0.97	0.98
Mix1	41.86	44.11	0.99	0.99
Mix2	41.41	40.90	0.99	0.99

sparse noise in the problem formulations.

The fourth set of experiments was carried out to check the evolution of the abundance maps with iterations. Figure 7 shows one of the abundance maps after every few iterations. Since all abundance maps had the same behavior, therefore evolution of only one abundance map is shown. It can be observed that after two iterations, there are many endmembers visible in the image. After 15 iterations, relevant endmembers has been found and both kinds of noise have got reduced.

The fifth set of experiments shows the estimation of sparse noise. The proposed formulation in (8) estimates sparse noise term S because S is not known apriori. Figure 8 shows how line strips are estimated as part of sparse noise term as iterations increases. It shows that the inclusion of sparse noise term helps in handling unmixing problem in the presence of

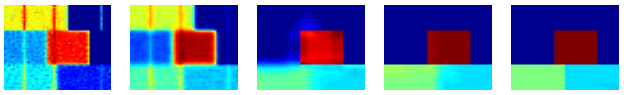

2 iterations 5 iterations 15 iterations 30 iterations 50 iterations

Fig. 7. Effect of Iterations on Abundances

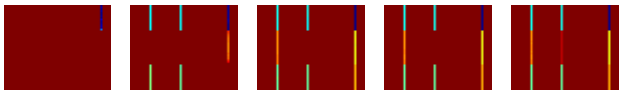

5 iterations 10 iterations 20 iterations 30 iterations 50 iterations

Fig. 8. Noise estimation

line strips.

The sixth set of experiments was carried out to check the convergence of proposed JSTV algorithm. The value of the objective function in (8) is plotted against the number of iterations. Figure 9 shows how objective function value decay to a locally optimal value. It can be deduced that fifty iterations are sufficient to reach the approximate solution; therefore, we can set maximum iterations to fifty.

The seventh set of experiments was carried out to compare time requirements of various algorithms. Public domain implementations of SR, CLSR, and SRTV available from [38] were utilized. Table IV summarizes the time taken by various algorithms on the first synthetic image with Gaussian noise of 30 dB SNR and three vertical lines. Time was calculated on Intel Core i7 machine having 8 GB RAM with Linux operating system and Matlab2013a software. These time requirements shown in Table IV are implementation dependent and may

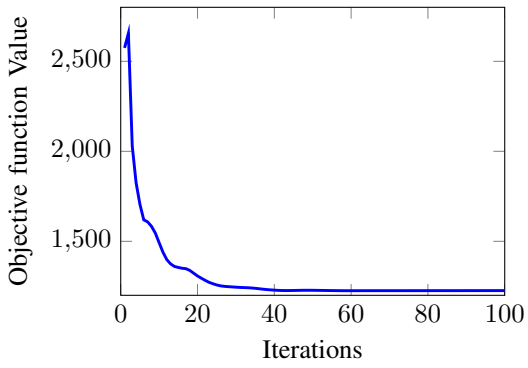

Fig. 9. Convergence of proposed JSTV algorithm

TABLE IV
COMPARISON OF TIME REQUIREMENTS

	SR	CLSR	SRTV	SBJS	SBTV	JSTV
Time (sec)	5.42	6.71	18.23	5.12	12.28	12.92

vary from machine to machine. Major time was consumed in approximating the least-square problem in each iteration and matrix-matrix multiplications. It can be noted that proposed JSTV can also be parallelized and applied on overlapping blocks simultaneously. Time reported is averaged over ten experiments.

C. Evaluation Metric

All the experimental results were quantified using two metrics namely peak signal to noise ratio (PSNR) and structural similarity index measure (SSIM) [39]. PSNR between original image x and reconstructed image y was calculated as:

$$\text{PSNR} = 10\log_{10}\left(\frac{\max(x)^2}{\text{MSE}}\right).$$

The PSNR value for a hyperspectral image was calculated as the average of the sum of PSNR value for each band. The exact reconstruction will lead to the maximum value of PSNR as infinite. Higher the PSNR value better is the reconstruction quality. The SSIM [39] is based on luminance (l), contrast (c), and structure (s) terms, calculated as follows:

$$\begin{aligned}\text{SSIM}(x,y) &= l(x,y)^\alpha \cdot c(x,y)^\beta \cdot s(x,y)^\gamma \\ l(x,y) &= \frac{2\mu_x\mu_y + c_1}{\mu_x^2 + \mu_y^2 + c_1} \\ c(x,y) &= \frac{2\sigma_x\sigma_y + c_2}{\sigma_x^2 + \sigma_y^2 + c_2} \\ s(x,y) &= \frac{2\sigma_{xy} + c_3}{\sigma_x\sigma_y + c_3}\end{aligned}$$

where c_1, c_2, c_3 are constants and parameters α, β, γ were set to one. $\mu_x, \mu_y, \sigma_x, \sigma_y$ are mean and standard deviations for images x and y. σ_{xy} is cross-covariance between x, and y. SSIM value is normalized between zero and one where maximum value of one indicate exact reconstruction.

D. Real Data Experiments

The real data experiments were done on a portion of Jasper image as described in data description section. All 224 bands were considered during experiments. The four major abundances maps estimated by various algorithms are shown in Fig. 10. Visually we can compare the quality of estimating these abundances with the original image shown in Fig. 2. We can observe from Fig. 10(a) and 10(b) that SR and CLSR algorithms resulted in noisy abundance map corresponding to water endmember. Similarly, the abundance map for road related pixels also shows some other materials. The proposed JSTV method has resulted in comparatively cleaner abundance maps as shown in Fig 10(f).

We have also compared denoising results by various algorithm since Jasper image have some noisy bands. Figure 11 shows bands 1 of Jasper image as well as its zoom portion over a small rectangular area. It can be observed from zoomed portions that proposed JSTV algorithm resulted in comparatively cleaner image.

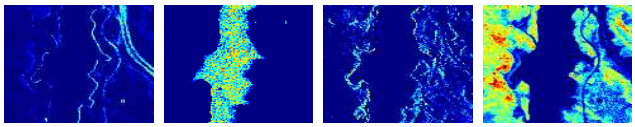

(a) Abundance maps estimated by SR

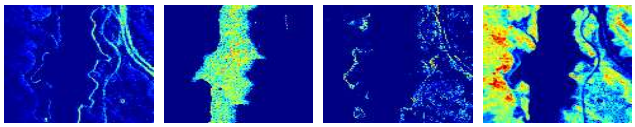

(b) Abundance maps estimated by CLSR

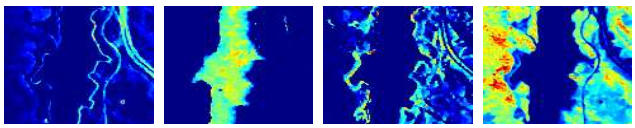

(c) Abundance maps estimated by SRTV

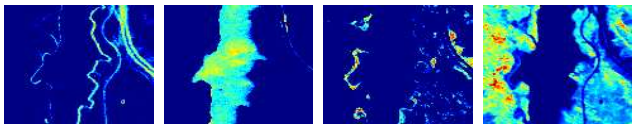

(d) Abundance Maps estimated by SBJS

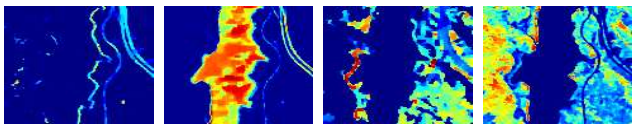

(e) Abundance maps estimated by SBTV

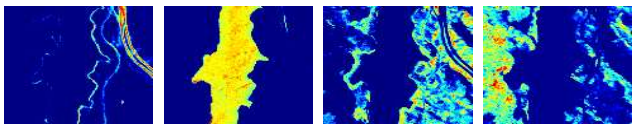

(f) Abundance maps estimated by JSTV

Fig. 10. Four major abundance maps estimated by different algorithms. Left to right : abundance maps corresponding to road, water, soil, and vegetation.

V. CONCLUSIONS

In this work, we have proposed a new approach for hyperspectral unmixing. This approach exploits joint sparsity as well as the piece-wise smoothness of abundance maps in the generic noise model which explicitly account for sparse noise. Experimental results suggest the advantage of proposed method over existing methods. Simultaneous utilization of both total-variation regularization and joint-sparse regularization is not redundant as both achieve different goals. Total variation regularization has explored smoothness of abundance maps whereas joint-sparsity exploit the fact that an endmember if present, shall be present at various locations in the same area.

This work utilized existing USGS spectral library for spectral signatures. The spectral signatures in the existing library can differ from the spectral signatures present in the

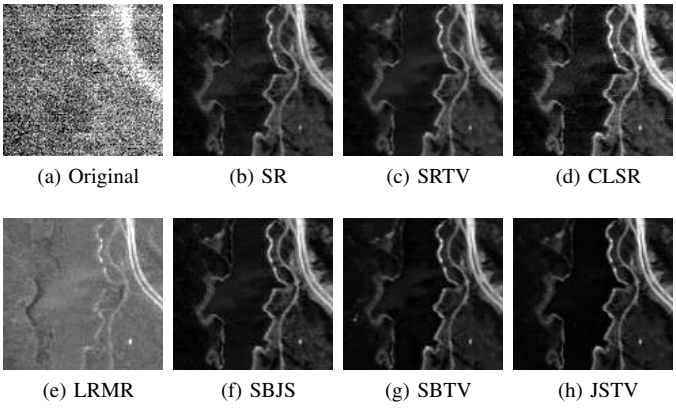

(a) Original (b) SR (c) SRTV (d) CLSR

(e) LRMR (f) SBJS (g) SBTV (h) JSTV

Fig. 11. Denoising results on Jasper image obtained by different algorithms. Top row: Band 1 denoised by various algorithms. Bottom row: zoomed in portion of the same band marked with white square.

image. Also, it is possible that real images have endmembers whose spectral signatures are not present in existing libraries; therefore, we will extend the work to derive the endmember signatures directly from the hyperspectral image.

REFERENCES

[1] J. Chi and M. M. Crawford, "Spectral Unmixing-Based Crop Residue Estimation Using Hyperspectral Remote Sensing Data: A Case Study at Purdue University," *IEEE J. Sel. Top. Appl. Earth Obs. Remote Sens.*, vol. PP, no. 99, pp. 1–10, 2014.

[2] M. Hedegaard, C. Matthäus, S. r. Hassing, C. Krafft, M. Diem, and J. Popp, "Spectral unmixing and clustering algorithms for assessment of single cells by Raman microscopic imaging," *Theor. Chem. Acc.*, vol. 130, no. 4-6, pp. 1249–1260, 2011.

[3] I. Dopido, A. Villa, A. Plaza, and P. Gamba, "A Quantitative and Comparative Assessment of Unmixing-Based Feature Extraction Techniques for Hyperspectral Image Classification," *IEEE J. Sel. Top. Appl. Earth Obs. Remote Sens.*, vol. 5, no. 2, pp. 421–435, 2012.

[4] A. Ertürk, "Enhanced Unmixing-Based Hyperspectral Image Denoising Using Spatial Preprocessing," *IEEE J. Sel. Top. Appl. Earth Obs. Remote Sens.*, vol. 8, no. 6, pp. 2720–2727, 2015.

[5] S. Delalieux, P. J. Zarco-Tejada, L. Tits, M. A. J. Bello, D. S. Intrigliolo, and B. Somers, "Unmixing-based fusion of hyperspatial and hyperspectral airborne imagery for early detection of vegetation stress," *IEEE J. Sel. Top. Appl. Earth Obs. Remote Sens.*, vol. 7, no. 6, pp. 2571–2582, 2014.

[6] Y. Gu, Y. Zhang, and J. Zhang, "Integration of spatial-spectral information for resolution enhancement in hyperspectral images," *IEEE Trans. Geosci. Remote Sens.*, vol. 46, no. 5, pp. 1347–1358, 2008.

[7] J. M. Bioucas-dias, A. Plaza, N. Dobigeon, M. Parente, Q. Du, P. Gader, and J. Chanussot, "Hyperspectral Unmixing Overview: Geometrical , Statistical , and Sparse Regression-Based Approaches," *IEEE J. Sel. Top. Appl. Earth Obs. Remote Sens.*, vol. 5, no. 2, pp. 354–379, 2012.

[8] R. Heylen, M. Parente, and P. Gader, "A review of nonlinear hyperspectral unmixing methods," *IEEE J. Sel. Top. Appl. Earth Obs. Remote Sens.*, vol. 7, no. 6, pp. 1844–1868, 2014.

[9] J. W. Boardman, "Automating spectral unmixing of AVIRIS data using convex geometry concepts," in *Summ. 4th Annu. JPL Airborne Geosci. Work.*, 1993, pp. 11–14.

[10] M. E. Winter, "N-FINDR: an algorithm for fast autonomous spectral end-member determination in hyperspectral data," in *SPIE Int. Symp. Opt. Sci. Eng. Instrum.*, 1999, pp. 266–275.

[11] L. Miao and H. Qi, "Endmember extraction from highly mixed data using minimum volume constrained nonnegative matrix factorization," *IEEE Trans. Geosci. Remote Sens.*, vol. 45, no. 3, pp. 765–777, 2007.

[12] D. Cerra, M. Rupert, and P. Reinartz, "Noise Reduction in Hyperspectral Images Through Spectral Unmixing," *IEEE Geosci. Remote Sens. Lett.*, vol. 11, no. 1, pp. 109–113, 2014.

[13] Z. Zhou, X. Li, J. Wright, E. Candès, and Y. Ma, "Stable Principal Component Pursuit," in *IEEE Int. Symp. Inf. Theory*, 2010, pp. 1518–1522.

[14] H. Zhang, W. He, L. Zhang, H. Shen, and Q. Yuan, "Hyperspectral Image Restoration Using Low-Rank Matrix Recovery," *IEEE Trans. Geosci. Remote Sens.*, vol. PP, no. 99, pp. 1–15, 2013.

[15] J. V. Shi, A. C. Sankaranarayanan, C. Studer, and R. G. Baraniuk, "Video compressive sensing for dynamic MRI," *BMC Neurosci.*, vol. 13, no. Suppl 1, p. P183, 2012.

[16] L. I. Rudin, S. Osher, and E. Fatemi, "Nonlinear Total Variation Based Noise Removal Algorithms," *Phys. D Nonlinear Phenom.*, vol. 60, no. 1, pp. 259–268, 1992.

[17] T. Goldstein and S. Osher, "The Split Bregman Method for L1-Regularized Problems," *SIAM J. Imaging Sci.*, vol. 2, no. 2, pp. 323–343, Jan. 2009.

[18] J. M. Bioucas-dias and M. A. T. Figueiredo, "Alternating Direction Algorithms for Constrained Sparse Regression: Application to Hyperspectral Unmixing," in *Work. Hyperspectral Image Signal Process. Evol. Remote Sens.*, 2010, pp. 1–4.

[19] M.-d. Iordache, J. M. Bioucas-dias, and A. Plaza, "Total Variation Spatial Regularization for Sparse Hyperspectral Unmixing," *IEEE Trans. Geosci. Remote Sens.*, vol. 50, no. 11, pp. 4484–4502, 2012.

[20] ——, "Collaborative Sparse Regression for Hyperspectral Unmixing," *IEEE Trans. Geosci. Remote Sens.*, vol. 52, no. 1, pp. 341–354, 2014.

[21] M.-D. Iordache, J. M. Bioucas Dias, and A. Plaza, "Sparse Unmixing of Hyperspectral Data," *IEEE Trans. Geosci. Remote Sens.*, vol. 49, no. 6, pp. 2014–2039, 2011.

[22] Q. Qu, N. M. Nasrabadi, and T. D. Tran, "Abundance Estimation for Bilinear Mixture Models via Joint Sparse and Low-Rank Representation," *IEEE Trans. Geosci. Remote Sens.*, vol. 52, no. 7, pp. 4404–4423, 2014.

[23] D. Donoho, "Compressed sensing," *IEEE Trans. Inf. Theory*, vol. 52, no. 4, pp. 1289–1306, Apr. 2006.

[24] E. Candes, J. Romberg, and T. Tao, "Stable Signal Recovery from Incomplete and Inaccurate Measurements," *Commun. Pure Appl. Math.*, vol. 59, no. 8, pp. 1207–1223, 2006.

[25] B. K. Natarajan, "Sparse approximate solutions to linear Systems," *SIAM J. Comput.*, vol. 24, no. 2, pp. 227–234, 1995.

[26] J. A. Tropp and A. C. Gilbert, "Signal Recovery From Random Measurements Via Orthogonal Matching Pursuit," *IEEE Trans. Inf. Theory*, vol. 53, no. 12, pp. 4655–4666, 2007.

[27] D. L. Donoho, Y. Tsaig, I. Drori, and J. L. Starck, "Sparse solution of underdetermined systems of linear equations by stagewise orthogonal matching pursuit," *IEEE Trans. Inf. Theory*, vol. 58, no. 2, pp. 1094–1121, 2012.

[28] D. Needell and J. a. Tropp, "CoSaMP: Iterative signal recovery from incomplete and inaccurate samples," *Appl. Comput. Harmon. Anal.*, vol. 26, no. 3, pp. 301–321, 2009.

[29] E. Van Den Berg and M. P. Friedlander, "Probing the pareto frontier for basis pursuit solutions," *SIAM J. Sci. Comput.*, vol. 31, no. 2, pp. 890–912, 2008.

[30] A. Beck and M. Teboulle, "A Fast Iterative Shrinkage-Thresholding Algorithm for Linear Inverse Problems," *SIAM J. Imaging Sci.*, vol. 2, no. 1, pp. 183–202, Jan. 2009.

[31] S. Becker, J. Bobin, and E. J. Candes, "NESTA : A Fast and Accurate First-Order Method for Sparse Recovery," *SIAM J. Imaging Sci.*, vol. 4, no. 1, pp. 1–39, 2011.

[32] W. Yin, S. Osher, D. Goldfarb, and J. Darbon, "Bregman Iterative Algorithms for L1-minimization with Applications to Compressed Sensing," *SIAM J. Imaging Sci.*, vol. 1, no. 1, pp. 143–168, 2008.

[33] M. A. T. Figueiredo and R. D. Nowak, "An EM Algorithm for Wavelet-Based Image Restoration," *IEEE Trans. Image Process.*, vol. 12, no. 8, pp. 906–916, 2003.

[34] M. A. Saunders, "Solution of Sparse Rectangular Systems Using LSQR and CRAIG," *BIT Numer. Math.*, vol. 35, no. 4, pp. 588–604, 1995.

[35] USGS, "Spectral library," http://speclab.cr.usgs.gov/spectral-lib.html, last accessed : Nov. 30, 2015.

[36] S. Grupo de Inteligencia Computacional, Universidad del Pas Vasco / Euskal Herriko Unibertsitatea (UPV/EHU), "Hyperspectral Imagery Synthesis (EIAs) toolbox." http://www.ehu.es/ccwintco/index.php/Hyperspectral_Imagery_Synthesis_tools_for_MATLAB, last accessed : Nov. 30, 2015.

[37] AVIRIS, "Jasper Image," http://www.cossa.csiro.au/hswww/Overview.htm, last accessed : Nov. 30, 2015.

[38] J. B. Dias, "source codes of SR, SRTV, CLSR," http://www.lx.it.pt/%7ebioucas/code.htm, last accessed : Nov. 30, 2015.

[39] Z. Wang, A. C. Bovik, H. R. Sheikh, and E. P. Simoncelli, "Image quality assessment: from error visibility to structural similarity." *IEEE Trans. Image Process.*, vol. 13, no. 4, pp. 600–12, Apr. 2004.